Scattering of Electromagnetic Pulses by Simple-Shaped Targets with Radar Cross Section Modified by a Dielectric Coating

Hans C. Strifors, *Member, IEEE,* and Guillermo C. Gaunaurd, *Senior Member, IEEE*

***Abstract*— We study the scattering interaction of electromagnetic pulses with a spherical target. The target is a perfectly conducting sphere coated with a thin dielectric layer. Two different hypothetical materials are specified: a lossy dielectric and a dielectric that also has magnetic losses. The monostatic radar cross section (RCS) is computed in each case and we examine the influence of the coating on the RCS. In particular, we compare the RCS of the coated sphere with the (normalized) backscattered power when a large perfectly conducting flat plate coated with the same dielectric layer is illuminated at normal incidence by the same waveform. In particular, we find that except for frequencies below those within the efficiency band of the absorbent material, the normalized RCS of the coated sphere agrees well with the power reflection coefficient of the plate covered with the same kind of coating. For low-frequency incidences, the peaks and dips in the RCS are more prominent for the coated target than they are for the bare one. Analyzing the response of the spherical targets in the combined time-frequency domain we demonstrate that the coating itself, although reducing the RCS could introduce additional resonance features in the target's signature at low frequencies that could be used for target recognition purposes. This observation is also confirmed by a study of the bistatic RCS of these coated objects, which we have displayed in various color graphs.**

***Index Terms*—Electromagnetic scattering, radar cross sections.**

I. Introduction

THE determination of radar cross-sections (RCS's) of targets of simple shape has received much attention and is now a well-studied problem area [1], [2]. The analytical treatment of scattering by penetrable spherical or cylindrical targets has, in general, considered material compositions of the targets that produce only small amounts of absorption of the incident signal power, if any at all. When the material composition of the target includes a radar absorbing material (RAM), complex-valued arguments enter the Bessel functions in the partial wave solution of the scattered field. This causes the break down of conventional evaluation algorithms [3], which require stable recurrence relations. By coating a given target with a thin layer of suitable electromagnetic properties, the RCS can be reduced and it is of interest to investigate the resulting radar cross-section reduction (RCSR). It is also of interest to investigate the effect of the RCSR on the scattering of pulses of short duration. We study the scattering interaction of ultrawide-band (UWB) electromagnetic pulses of short duration with a spherical target. The target is either a perfectly conducting sphere (for comparison) or such a sphere coated with a thin homogeneous dielectric (Dällenbach [1], [2]) layer.

For the dielectric layer, two different hypothetical materials and a single thickness are specified. It is an established procedure to specify the radar absorbing properties of a material by referring to its reflection characteristics when the material is in the shape of a plane layer of specified thickness, which is then applied on a metal (or perfectly conducting) backing. As it turns out in this study, the RCSR of a RAM-coated target of three-dimensional (3-D) shape cannot, in general, be determined from the properties of the RAM applied to a flat plate. Following the traditional procedure, we characterize each dielectric layer by computing the power reflection coefficient when a flat perfectly conducting plate coated with the layer is illuminated by a continuous wave (CW) at normal incidence in a selected frequency band. Each one of the coatings is then applied on the perfectly conducting sphere, the (monostatic) RCS is computed, and we compare it with the returned power from the coated plate normalized to that of the incident wave.

The analysis of returned echoes has been traditionally done in the frequency domain [1], [2], [4]–[8]. A recent method of processing echoes that is gaining acceptance is to analyze them in the *combined* time-frequency domain. This approach seems to offer more advantages because both the spectral content of the target response and its time evolution can be utilized for target recognition purposes. The identifying signature features of a target can be displayed in a general time-frequency-amplitude plot in 3-D space. Usually, projections of a number of contour levels of these 3-D surfaces are shown in the two-dimensional (2-D) time-frequency plane; e.g., [9]–[11]. However, contour plots tend to emphasize the gradient of a 3-D surface rather than the amplitude level. To emphasize the amplitude displayed in the surface plot of each time-frequency signature, the 3-D surface is shown in color using an arbitrary color scale and is projected to obtain a 2-D intensity image in the time-frequency plane. The evolution of the signature features is extracted by means of any of the many distributions that are members of the general bilinear class [12], [13]. This includes the distributions at-

Manuscript received October 20, 1995; revised January 12, 1998.

H. C. Strifors is with the National Defense Research Establishment, Stockholm, (FOA-6) S-172 90 Sweden.

G. C. Gaunaurd is with the Naval Surface Warfare Center, Carderock Division-Code 684, W. Bethesda, MD 20817 USA.

Publisher Item Identifier S 0018-926X(98)06868-9.

tributed to Wigner, Ville, Margenau-Hill, Kirkwood-Rihaczek, Choi-Williams, etc., each with its own characteristics, though sharing the essential properties of time-frequency distributions. As we demonstrated earlier [9], [10], the target resonances that can be extracted from an echo backscattered from a target when a short pulse (from an impulse radar) is incident on it can be used to identify the target. These transient interactions were preliminary analyzed in the time-frequency domain using a pseudo-Wigner distribution (PWD) [9]. The advantages of the PWD become more obvious when it is compared with the standard spectrum (or the RCS) of the considered echo returns. Thus, using a PWD we extend the analysis to the time-frequency domain of the target by examining the backscattered echo when each of these spherical targets is illuminated by a short broad-band pulse resembling the one that was used in [6]. The computational machinery illustrated here with the PWD can be implemented with *any* of the other distributions members of the bilinear class [12]–[14]. It can be stated that *all* bilinear distributions can be viewed as smoothed versions of the WD with their amount of smoothing determining the amount of suppression of the cross-term interference and the loss of time-frequency concentration of features. Finally, we generate bistatic RCS plots of these coated objects for two pertinent polarizations using a suitable color scale and we use them to confirm observations already extracted from the time-frequency (i.e., PWD) plots.

II. Steady-State Scattering

A. Scattering from Spherical Targets

A steady-state continuous plane electromagnetic wave $E_{\mathbf{in}} = E_0 \exp[i(\omega t + kz)]$ polarized in the x direction is incident on the North pole (defined by the spherical coordinate $\theta = 0$) of a perfectly conducting sphere of radius a, where E_0 is the amplitude of the field, ω the angular frequency, and $k = \omega/c$ the wave number in the surrounding medium taken to be free-space. Henceforth, we use the notation $x \equiv ka = 2\pi a/\lambda$ for the nondimensional frequency, where λ is the wavelength in free-space.

The scattered electric far field at the distance r ($r \gg a$) from the origin of the sphere can be written in the form [1], [4], [7] (cf. Fig. 1)

$$\mathbf{E}_{sc}(\theta, \phi, x) = E_0 \frac{e^{i(\omega t - kr)}}{kr} \cdot [\mathbf{e}_\theta S_1(\theta, x)\cos\phi - \mathbf{e}_\phi S_2(\theta, x)\sin\phi] \quad (1)$$

where θ and ϕ are the colatitude and azimuth angles, respectively, $\mathbf{e}_\theta$ and $\mathbf{e}_\phi$ unit vectors in these directions, and

$$\begin{Bmatrix} S_1(\theta, x) \\ S_2(\theta, x) \end{Bmatrix} = \frac{1}{i}\sum_{n=1}^{\infty}(-1)^n \frac{2n+1}{n(n+1)}\left[A_n(x)\begin{Bmatrix} \pi_n(\theta) \\ \tau_n(\theta) \end{Bmatrix} + B_n(x)\begin{Bmatrix} \tau_n(\theta) \\ \pi_n(\theta) \end{Bmatrix}\right]. \quad (2)$$

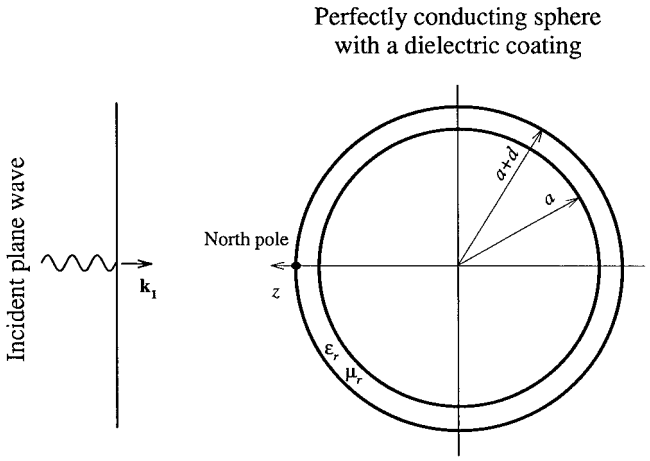

Fig. 1. Scattering geometry for plane wave incidence on a perfectly conducting sphere with a dielectric coating.

Here, the functions $\pi_n(\theta)$ and $\tau_n(\theta)$ are defined by

$$\pi_n(\theta) = \frac{P_n^1(\cos\theta)}{\sin\theta}, \quad \tau_n(\theta) = \frac{dP_n^1(\cos\theta)}{d\theta} \quad (3)$$

$P_n^1(\cdot)$ denoting the associated Legendre functions of first kind, first order, and nth degree, and the scattering coefficients $A_n(x)$ and $B_n(x)$ are given by

$$A_n(x) = -\frac{\psi_n(x)}{\zeta_n(x)}, \quad B_n(x) = \frac{\psi_n'(x)}{\zeta_n'(x)} \quad (4)$$

where the Sommerfeld functions $\psi_n(x) \equiv x\, j_n(x)$ and $\zeta_n(x) \equiv x\, h_n^{(2)}(x)$ are defined by the spherical Bessel functions of the first kind and the spherical Hankel functions of the second kind, respectively.

The (normalized) radar cross section (RCS) is then defined by

$$\frac{\sigma(\theta, \phi, x)}{\pi a^2} \equiv \lim_{r\to\infty}\left(\frac{2r}{a}\frac{|\mathbf{E}_{sc}(\theta, \phi, x)|}{|\mathbf{E}_{\mathbf{in}}(x)|}\right)^2 = |f_\infty(\theta, \phi, x)|^2 \quad (5)$$

where the dependence on the angles θ and ϕ are emphasized and the form-function $f_\infty(\theta, \phi, x)$ can be read off from (1)–(5). We note that the monostatic (backscattering) case is defined by $\theta = 0$.

When the target is the above perfectly conducting sphere of radius a with a dielectric coating of thickness d applied on it, the scattering coefficients (4) assume forms given in [7], though slightly modified because the coating is here assumed to be magnetic. In terms of the relative dielectric permittivity and magnetic permeability of the coating layer, the index of refraction, the relative impedance, and admittance are defined by $m_1 = \sqrt{\varepsilon_r \mu_r}$, $Z_1 = \sqrt{\mu_r/\varepsilon_r}$, and $Y_1 = \sqrt{\varepsilon_r/\mu_r}$. These quantities are, in general, functions of the angular frequency ω. The arguments that occur in the Sommerfeld functions defining the form function in this case are $x \equiv k(a+d)$, $x_1 \equiv k_1(a+d) = m_1 x$, and $x_2 \equiv k_1 a = m_1 x a/(a+d)$, where $k_1 = m_1 k$ is the wave number in the dielectric coating of

refractive index m_1. The scattering coefficients then assume the forms

$$A_n = -\frac{P_n(x) - T_n(x)Q_n(x)}{R_n(x) - T_n(x)S_n(x)},$$
$$B_n = \frac{\tilde{P}_n(x) - \tilde{T}_n(x)\tilde{Q}_n(x)}{\tilde{R}_n(x) - \tilde{T}_n(x)\tilde{S}_n(x)} \tag{6}$$

where the ten functions $P_n(x)$, $Q_n(x)\cdots$ are given by

$$\begin{aligned}
P_n(x) &= \psi_n(x_1)\,\psi_n'(x) - Y_1\,\psi_n(x)\,\psi_n'(x_1)\\
Q_n(x) &= \zeta_n(x_1)\,\psi_n'(x) - Y_1\,\psi_n(x)\,\zeta_n'(x_1)\\
R_n(x) &= \psi_n(x_1)\,\zeta_n'(x) - Y_1\,\zeta_n(x)\,\psi_n'(x_1)\\
S_n(x) &= \zeta_n(x_1)\,\zeta_n'(x) - Y_1\,\zeta_n(x)\,\zeta_n'(x_1)\\
T_n(x) &= \psi_n(x_2)\,/\,\zeta_n(x_2)\\
\tilde{P}_n(x) &= \psi_n(x_1)\,\psi_n'(x) - Z_1\,\psi_n(x)\,\psi_n'(x_1)\\
\tilde{Q}_n(x) &= \zeta_n(x_1)\,\psi_n'(x) - Z_1\,\psi_n(x)\,\zeta_n'(x_1)\\
\tilde{R}_n(x) &= \psi_n(x_1)\,\zeta_n'(x) - Z_1\,\zeta_n(x)\,\psi_n'(x_1)\\
\tilde{S}_n(x) &= \zeta_n(x_1)\,\zeta_n'(x) - Z_1\,\zeta_n(x)\,\zeta_n'(x_1)\\
\tilde{T}_n(x) &= \psi_n'(x_2)/\zeta_n'(x_2).
\end{aligned} \tag{7}$$

B. E- and H-Plane Scattering

We consider two particular cases of polarization, namely those defined by $\phi = 0$ and $\phi = \pi/2$, which are referred to as E-plane and H-plane (bistatic) scattering, respectively. The case of E-plane (or H-plane) scattering is defined by the incident E-field (or H-field) being parallel to the plane spanned by the direction of incidence and the scattering direction θ. Only in these two cases are the scattered electromagnetic far fields parallel to the incident electromagnetic field for any angle θ and any frequency x. The scattered E-field (polarized in the plane of the incident E-field) is in these two cases given by

$$\begin{aligned}
\begin{Bmatrix} \mathbf{E}_{Esc}(\theta, x) \\ \mathbf{E}_{Hsc}(\theta, x) \end{Bmatrix} &= E_0 \frac{e^{i(\omega t - kr)}}{kr} \begin{Bmatrix} S_1(\theta, x)\mathbf{e}_\theta \\ -S_2(\theta, x)\mathbf{e}_\phi \end{Bmatrix}\\
&= E_0 \frac{a}{2r} e^{i(\omega t - kr)} \begin{Bmatrix} f_\infty(\theta, \phi = 0, x)\mathbf{e}_\theta \\ f_\infty(\theta, \phi = \pi/2, x)\mathbf{e}_\phi \end{Bmatrix}
\end{aligned} \tag{8}$$

respectively, where E-plane or H-plane scattering is indicated by the index and the unit vectors are located in the xz plane.

C. Bessel functions of Complex-Valued Arguments

A distinguishing property of dielectric coatings used for reducing the RCS of objects is that the index of refraction is a *complex-valued* function of the frequency due to a complex permittivity or permeability or both. The presence of complex arguments, often with a large imaginary part in the form function, severely restricts successful numerical evaluation using traditional algorithms for the Bessel functions since the ordinary recurrence relations become unstable. To surmount the difficulties, we use an algorithm for calculating the spherical Bessel functions of the first kind that was developed by Lentz [15], [16]. This algorithm is based on a continued fraction representation of the ratios $j_{n-1}(z)/j_n(z)$. The continued fraction approach could also be used for computing the spherical Bessel functions of the second kind. We found, however, that the corresponding continued fraction representation of the ratios $y_{n-1}(z)/y_n(z)$ of the spherical Bessel functions of the second kind [15] is not stable enough to be computed with the numerical precision available in a personal computer (PC). Instead, the spherical Bessel functions of the second kind and the spherical Hankel functions of the second kind are calculated using the cross products [17, eq. (10.1.31)]

$$\begin{aligned}
y_n(z) &= [j_n(z)y_{n-1}(z) - z^{-2}]/j_{n-1}(z)\\
h_n^{(2)}(z) &= [j_n(z)h_{n-1}^{(2)}(z) + iz^{-2}]/j_{n-1}(z)
\end{aligned} \tag{9}$$

where the latter equation is a reformulation of the former using the definition of the spherical Hankel function [17, eq. (10.1.1)]. These calculations can then be conveniently performed using a PC. The recurrence formula given by $(9)_1$ was, in fact, recommended by Lentz [15] for calculations of the spherical Bessel function of the second kind. The recurrence formula for the spherical Hankel function given by $(9)_2$ has been tested by us in several instances and found to be stable and accurate at all occasions. We remark that in scattering applications where the absorption of incident signal power is large and the scattered energy quite small within a given frequency band, it turns out that the modulus of the pertinent spherical Hankel function (the second kind in our formulation) is also quite small in that band. As a consequence, the accurate calculation of the spherical Hankel function using the ordinary definition in terms of the spherical Bessel functions of first and second kind (viz., $h_n^{(2)} \equiv j_n - iy_n$) would require a large number of significant digits. This is because in many cases of practical interest the spherical Hankel function will come out as an exceedingly small difference of the spherical Bessel functions resulting in ruinous loss of accuracy.

D. Normal Incidence on a Coated Flat Plate

We consider a perfectly conducting plate (of infinite extent) coated by a homogeneous dielectric layer of thickness d with a CW illuminating its surface at normal incidence. It can be shown that the reflection coefficient in this case assumes the form [2]

$$R = e^{i2kd}\frac{1 - Y_1 - (1 + Y_1)e^{-i2k_1 d}}{1 + Y_1 - (1 - Y_1)e^{-i2k_1 d}}. \tag{10}$$

The modulus of the normalized reflected power is then given by the "power reflection coefficient" $|R|^2$.

III. Transient Scattering

We generalize the analysis to pulsed incidences [7], [9] by introducing a Fourier transform pair $g(t) \leftrightarrow G(\omega)$, where $g(t)$ is the incident pulse and $G(\omega)$ its spectrum

$$\begin{aligned}
G(\omega) &= \int_{-\infty}^{+\infty} g(t)e^{-i\omega t}dt \longleftrightarrow g(t)\\
&= \frac{1}{2\pi}\int_{-\infty}^{+\infty} G(\omega)e^{i\omega t}d\omega.
\end{aligned} \tag{11}$$

The scattered electric far field can then be shown to assume the form [7]

$$\begin{Bmatrix}\mathbf{E}_{Esc}(\theta,\,t)\\ \mathbf{E}_{Hsc}(\theta,\,t)\end{Bmatrix} = E_0\frac{c}{r}\frac{1}{2\pi}\int_{-\infty}^{+\infty} G(\omega) \cdot\begin{Bmatrix} S_1(\theta,\,\omega)\,\mathbf{e}_\theta\\ -S_2(\theta,\,\omega)\,\mathbf{e}_\phi\end{Bmatrix} e^{i(\omega t-kr)}d\omega = E_0\frac{a}{2r}\frac{1}{2\pi}\int_{-\infty}^{+\infty} G(\omega) \cdot\begin{Bmatrix} f_\infty(\theta,\,\phi=0,\,\omega)\,\mathbf{e}_\theta\\ f_\infty(\theta,\,\phi=\pi/2,\,\omega)\,\mathbf{e}_\phi\end{Bmatrix} e^{i(\omega t-kr)}\,d\omega \tag{12}$$

where we remember that positive values are obtained for the arrival time at the observation point for scattered pulses if r is chosen to be larger than $2a$.

When using the discrete-time Fourier transform (DFT) [19] in numerical calculations where the incident pulse is given in the form of a discrete-time series, which is assumed periodic, the above formulation of the continuous-time Fourier transform pair is conveniently converted to

$$G(k) = \sum_{n=0}^{N-1} g(n)e^{-i(2\pi/N)kn} \longleftrightarrow g(n) = \frac{1}{N}\sum_{k=0}^{N-1} G(k)\,e^{i(2\pi/N)kn} \tag{13}$$

where the sequences $g(n)$ and $G(k)$ both contain N elements.

IV. Target Responses in the Joint Time-Frequency Domain

The analysis of the returned echoes has been traditionally done in the frequency domain [1], [2], [4]. A recent method of processing signals that has been gaining acceptance is to work in the *combined* time-frequency domain. This approach seems to give the largest amount of information since it can display the evolution of the identifying resonance features of the scatterer and their amplitudes as surfaces in a general time-frequency-amplitude plot in 3-D space. Usually, projections of a number of contour levels of these 3-D surfaces are shown in the 2-D time-frequency plane. The evolution of signature features is extracted by any of the many distributions that are members of the general bilinear class, [12]–[14]. The (auto-) Wigner distribution (WD) of the function $f(t)$

$$W_f(\omega,\,t) = \int_{-\infty}^{+\infty} f\Big(t+\frac{\tau}{2}\Big)\,f^*\Big(t-\frac{\tau}{2}\Big)\,e^{-i\omega\tau}d\tau = 2\int_{-\infty}^{+\infty} f(t+\tau)\,f^*(t-\tau)\,e^{-i2\omega\tau}d\tau \tag{14}$$

is a member of the general bilinear class that shares with some other time-frequency distributions the property of preserving the time and frequency energy marginals of a signal, i.e., integration of the WD over the frequency variable at a generic time (or over the time variable at a generic frequency) yields the signal's instantaneous power at that time (or energy density spectrum at that frequency) [14]. Another property of the WD, which is desirable for target recognition purposes, is its excellent ability of *concentrating* the features of a function in the combined time-frequency domain.

Digital evaluation of the WD of continuous-time functions requires a reformulation of (14) to its analogue for discrete-time functions. Existing algorithms for fast Fourier transform (FFT) can then be adapted to the discrete Wigner distribution. Analogous to $(13)_1$, the discrete-time version of $(14)_2$, for a sequence $f(n)$ containing N elements is

$$W_f(k,l) = 2\sum_{n=0}^{N-1} f(l+n)\,f^*(l-n)\,e^{-i(4\pi/N)kn} \tag{15}$$

where $k,\,l = 0,\,1,\,2,\,\cdots,\,N-1$ represent frequency and time, respectively, and $f(l+n-N)$ is substituted for $f(l+n)$ whenever $l+n>N$. Comparing (15) with $(13)_1$ shows that the WD is periodic with period π rather than 2π, as is the case for the DFT. Thus, aliasing is, in general, present in the WD even when the sampling rate satisfies the Nyquist criterion. An approach to avoid aliasing (which we will use here) is to use the "analytic function" when computing the WD. This function is defined by $f_a(n) = f(n) + i\hat{f}(n)$, where $f(n)$ is a given real-valued function and $\hat{f}(n)$ is the discrete Hilbert transform [19] of $f(n)$. When analytic functions are used, the distribution in (14) or (15) is often called the Wigner–Ville distribution.

Practical applications of the WD are limited by the presence of "cross-terms." The cross-terms attributed to the bilinear nature of the distribution, generate features that lie between two autocomponents and can have peak values larger than those of the autocomponents. However, using the analytic function $f_a(n)$ eliminates cross-terms between positive and negative frequency components. There is a tradeoff between high feature concentration in the time-frequency domain and the suppression of cross-terms interference that can be achieved using any kind of smoothing of the WD. Thus, it is possible to *suppress the remaining* cross-terms interference by weighting the function before evaluating the WD using a window function. This window function can be made to slide along the time axis with the instant t at which the WD is being evaluated. Different window functions will place different weights on the time segments of the time-varying function $f(t)$, which will yield different physical interpretations of the resulting pseudo-Wigner distribution (PWD). Another important property of the window function is that, if narrow enough, it suppresses the influence of noise on the PWD. If $w_f(t)$ is the window function, the PWD of $f(t)$ is

$$\tilde{W}_f(\omega,\,t) = 2\int_{-\infty}^{+\infty} f(t+\tau)\,f^*(t-\tau)\,w_f(\tau)\,w_f^*(-\tau) \cdot e^{-i2\omega\tau}d\tau \tag{16}$$

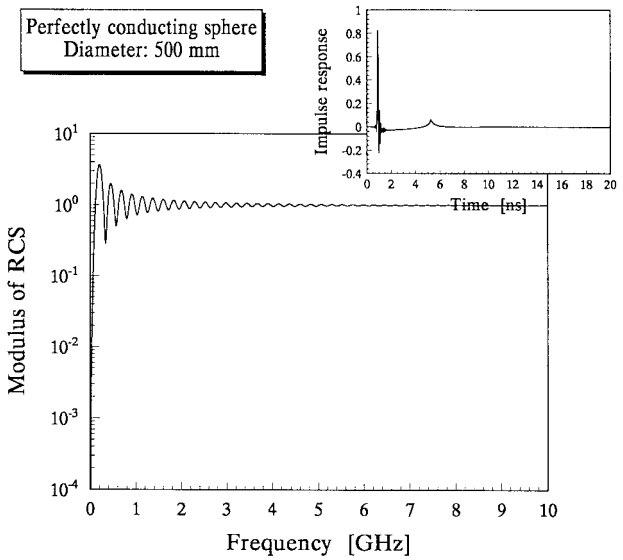

Fig. 2. Modulus of the RCS (main plot) and impulse response (insert plot) of a perfectly conducting sphere of diameter 500 mm.

and the corresponding discrete pseudo-Wigner distribution (DPWD) is given by

$$\tilde{W}_f(k,l) = 2\sum_{n=0}^{N-1} f(l+n)\, f^*(l-n)\, w_f(n) \cdot w_f^*(-n)\, e^{-i(4\pi/N)kn}. \tag{17}$$

A convenient window function is a Gaussian of the form $w_f(t) = \exp(-\alpha t^2)$, where α is a positive real number that controls the width of the time window.

V. Numerical Results

We examine the effect of dielectric coatings on the backscattered pulses returned by the target when the applied coatings are made of two different hypothetical materials. Coating "A" is a nonmagnetic (i.e., $\mu_r = 1$) lossy dielectric layer with relative permittivity $\varepsilon_r = 15 - 5i$ and thickness 5 mm and coating "B" has the magnetic permeability $\mu_r = 18 - 9i$, permittivity $\varepsilon_r = 20 - 10i$, and thickness 5 mm. The electromagnetic properties of the coating materials are assumed to be independent of the frequency in the broad band $0 \le f \le 10$ GHz, which is not an entirely realistic assumption. The assumption means that the energy dissipation (or absorption) is instantaneous and it is made here for convenience. Generally, the electromagnetic constitutive equations for dissipative materials are assumed to be functionals of the more realistic Volterra-integral type for which the Kramers–Krönig relations apply.

For comparison, we first compute the monostatic RCS of a perfectly conducting sphere of radius $a = 250$ mm in the frequency band $0 \le f \le 10$ GHz and the result is displayed in Fig. 2, main plot. Fig. 2, insert plot, displays the impulse response of the target. Fig. 3, main plot, displays the power reflection coefficient when a plate covered with coating A is illuminated at normal incidence, and the insert plot shows the response of the coated plate to an ideal impulse (i.e., a

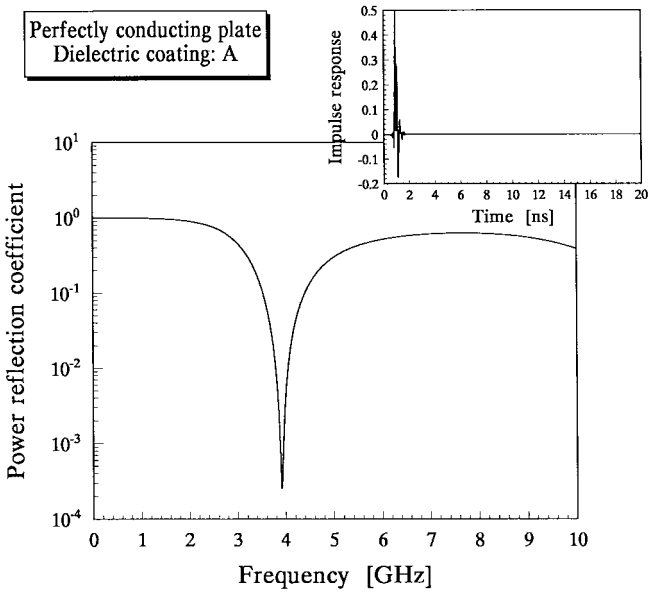

Fig. 3. Power reflection coefficient (main plot) and impulse response (insert plot) of a flat plate covered with coating A.

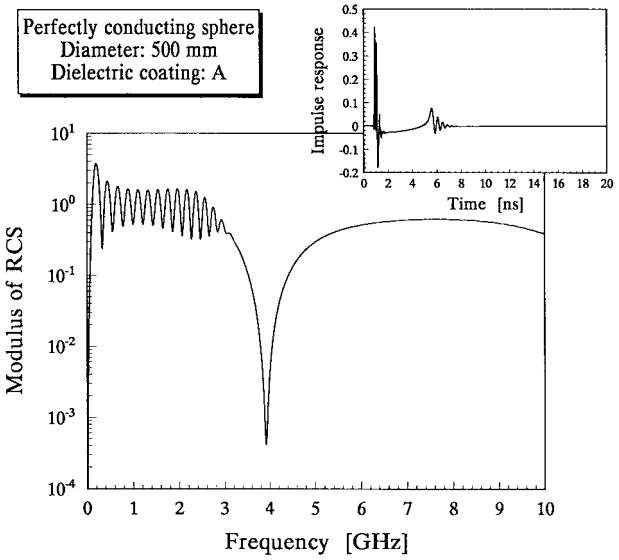

Fig. 4. Modulus of the RCS (main plot) and impulse response (insert plot) of a perfectly conducting sphere covered with coating A.

Dirac delta pulse). We notice the narrow absorption band of this type of coating, which has an echo reduction better than 30 dB within an extremely narrow band centered about 3.9 GHz. Fig. 4 (main plot) displays the monostatic RCS of a perfectly conducting sphere of radius $a = 250$ mm with the same type (viz. A) of coating applied. Comparing the main plots of Figs. 3 and 4 we see that the modulus of the RCS of the coated sphere agrees very well with the power reflection coefficient of the coated plate for frequencies above ~3 GHz. At lower frequencies the RCS exhibits the peaks and dips characteristic of the influence of the secondary surface-wave returns, which can be seen in the impulse response of the target (Fig. 4, insert plot) in the time interval $5 < t < 7$ ns. A closer examination of the lower-frequency portion of the RCS reveals that the RCS relative to the RCS of the uncoated sphere

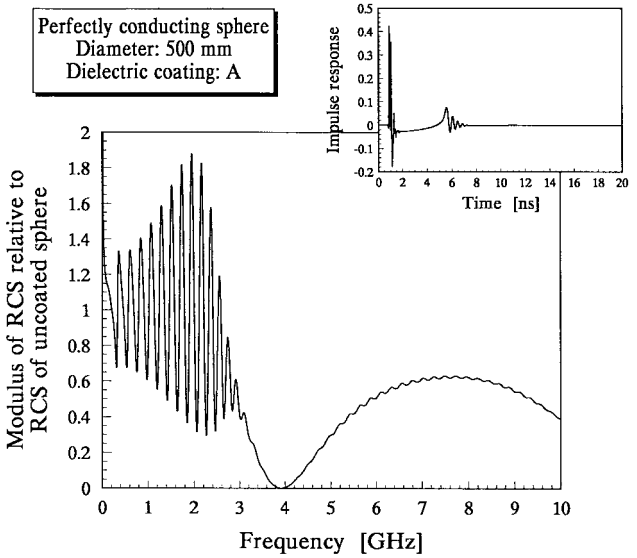

Fig. 5. Modulus of the RCS (main plot) of a perfectly conducting sphere covered with coating A relative to the RCS of the uncoated sphere.

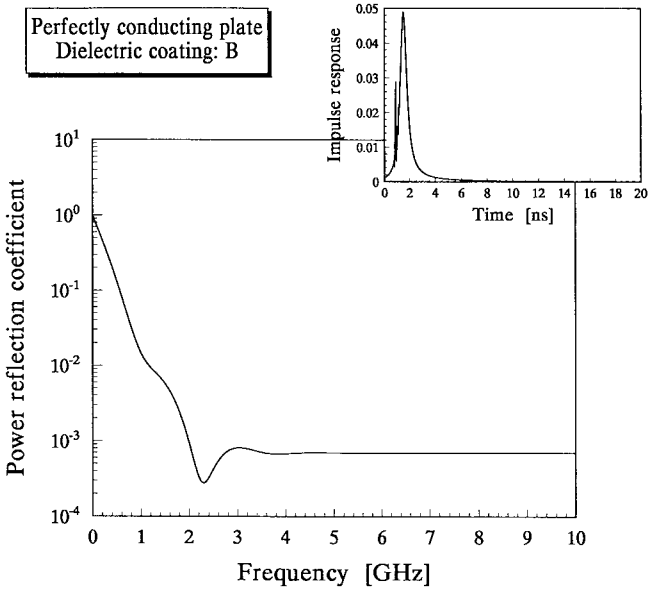

Fig. 6. Power reflection coefficient (main plot) and impulse response (insert plot) of a flat plate covered with coating B.

in Fig. 2 reaches peak values that are almost twice as large in a 1-GHz band around the frequency 2 GHz. Fig. 5, main plot, displays the modulus of the RCS of the coated sphere relative to the RCS of the uncoated sphere. We also notice that only a slight amount of RCSR (viz. a single dB, as is apparent from Fig. 2 main plot) is sufficient at higher frequencies for the contribution to the RCS from the secondary echo returns to be annihilated (cf. Fig. 4, main plot).

In the present work, all calculations of reflected power and RCS are carried out using 4096 equal frequency steps. To avoid aliasing errors each impulse response is computed from the respective electric field in the frequency domain after lowpass filtering has been performed using a second-order Butterworth filter with a cutoff frequency of 8.5 GHz and, since the time-domain functions should be real valued, the reversed complex conjugate sequence has been appended to the computed sequence. Fourier transforms (13) or pseudo-Wigner distributions (17) are then computed using the complete sequence of $N = 8192$ elements.

For comparison with the RCSR achieved with the aid of a coating with a broad efficiency band, we contrast these results with the corresponding results when coating B is applied to a plate and to a sphere of radius $a = 250$ mm, as displayed in Figs. 6 and 7 main plots, respectively. The power reflection coefficient of the coated plate (Fig. 6 main plot) is practically identical to the normalized RCS for the coated sphere (Fig. 7 main plot) when the frequency is larger than about 1 GHz and at lower frequencies the occurrence of peaks and dips in the RCS again reveals the influence of the secondary (i.e., "creeping wave") returns. The impulse response of the coated plate and the initial return of the impulse response of the coated sphere (Figs. 6 and 7 insert plots) have very low amplitudes compared with the cases displayed in Figs. 3 and 4. They can both be seen to be comprised of one (tiny) portion that has been reflected at the outer surface of the coating and another portion that has traveled round-trip through the dielectric layer with a time separation (viz. $\sim$0.63 ns) that corresponds to the speed of propagation in the layer (viz., $\sim$15.8 mm/ns). We remark that the agreement obtained between the power reflection coefficient and the RCS in broad frequency bands only holds when *normal incidence* on the coated plate and *monostatic* scattering by the coated sphere are compared. Fig. 8 main plot displays the modulus of the RCS of the sphere coated with layer B relative to that of the uncoated sphere. This relative RCS exhibits characteristics analogous to those obtained for coating A (cf. Fig. 5 main plot). Thus, for frequencies below the efficiency band of the coating, it acts as a lossless waveguide and intensifies the constructive and destructive interactions of the primary, specular return and the secondary (creeping) return that has circumnavigated the target. In this manner, the coating actually contributes to the RCS in several narrow frequency bands.

A theoretical model of the pulses being transmitted by an impulse radar can be conveniently obtained by filtering an ideal impulse using a Butterworth bandpass filter of suitable filter order and cutoff frequencies [9], [10]. To achieve a broadband, fictitious, but realistic, waveform for illuminating targets we select a filter of order six and cutoff frequencies of value 0.2 and 5.0 GHz. Fig. 9 displays the waveform (insert plot) and its spectrum (main plot) that results from this design. As the first target to be illuminated with the designed pulse we choose an *uncoated* perfectly conducting sphere of radius 250 mm. We compute the modulus of the PWD of the backscattered pulse using a window size specified by $\alpha = 0.5$ (ns)$^{-2}$ and we display it using the 3-D surface plot and its plane 2-D projection contour plot in Fig. 10. The lateral grid planes display the waveform and power density spectrum of the returned pulse using (unnumbered) linear scales. We contrast this PWD of the perfectly conducting sphere with the PWD for the same target when it is covered with coating A (or B) in Fig. 11 (or 12). The relative strength of the returned pulses

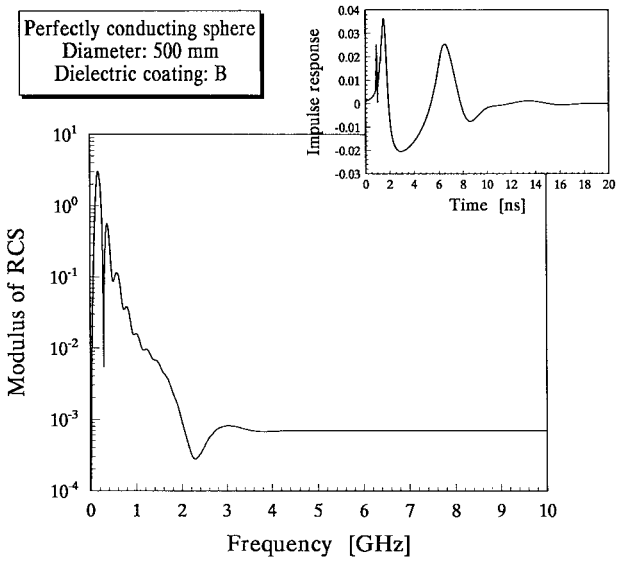

Fig. 7. Modulus of the RCS (main plot) and impulse response (insert plot) of a perfectly conducting sphere covered with coating B.

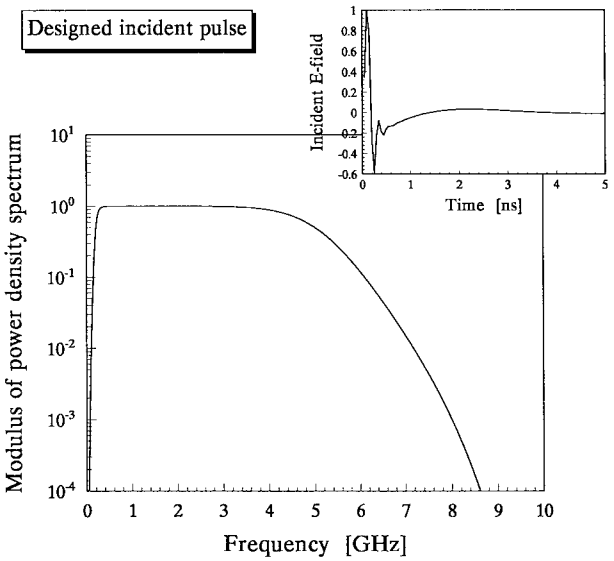

Fig. 9. The spectrum of the designed incident pulse (main plot) and its waveform (insert plot).

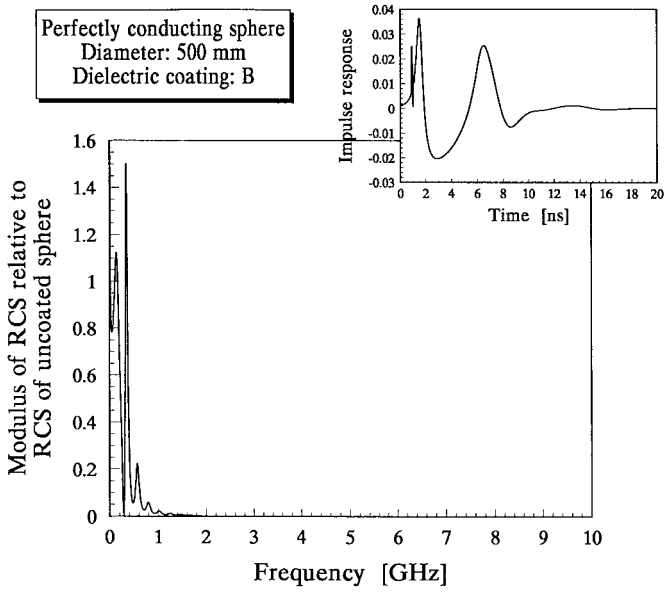

Fig. 8. Modulus of the RCS (main plot) of a perfectly conducting sphere covered with coating B relative to the RCS of the uncoated sphere.

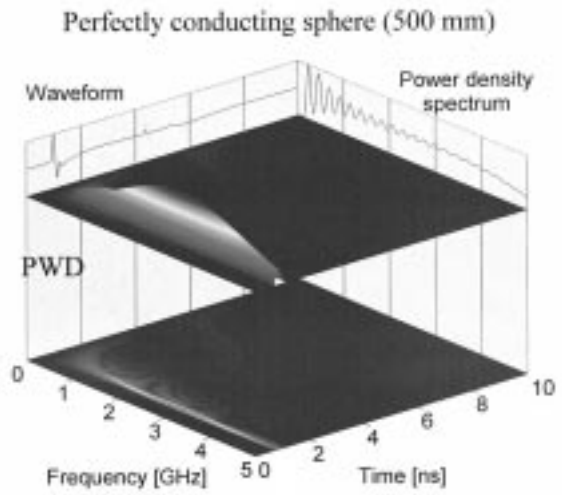

Fig. 10. Surface plot and its plane projection intensity image of the PWD together with the returned waveform and its power density spectrum when a perfectly conducting sphere is illuminated in monostatic mode by the designed incident pulse.

(best noticed in the impulse responses in Figs. 4 and 7 insert plots) are not evident from the PWD plots since arbitrary units are used for all plotted functions to more clearly exhibit the resonance features of the PWD's. We conclude from those PWD's that resonance features can be best extracted at low frequencies where, possibly, the RCSR is not strong enough to suppress the effect of the secondary echo returns on the RCS. Absorbing coatings have long been known to be ineffective at (sufficiently) low frequencies [20]. Our findings verify this point and further show that they can generate additional resonance features that may be used as identifying clues at those low frequencies [21]–[23]

Finally, we analyze bistatic RCS. Combining (5) and (8) for the E-plane and H-plane scattering cases, we obtain (normalized) cross-sections in these respective planes given by

$$\begin{Bmatrix} \sigma_{Esc}(\theta, x)/\pi a^2 \\ \sigma_{Hsc}(\theta, x)/\pi a^2 \end{Bmatrix} = \begin{Bmatrix} |f_\infty(\theta, \phi = 0, x)|^2 \\ |f_\infty(\theta, \phi = \pi/2, x)|^2 \end{Bmatrix} = \begin{Bmatrix} \left|\frac{2}{x} S_1(\theta, x)\right|^2 \\ \left|\frac{2}{x} S_2(\theta, x)\right|^2 \end{Bmatrix} \tag{18}$$

where $S_1(\theta, x)$ and $S_2(\theta, x)$ are given in (2)–(4) for the bare sphere. For the sphere covered with either coating, the coefficients A_n and B_n appearing in (2) are replaced by those in (6) and (7). These bistatic cross-sections are displayed in Figs. 13 and 14 for the bare sphere, in Figs. 15 and 16 for the

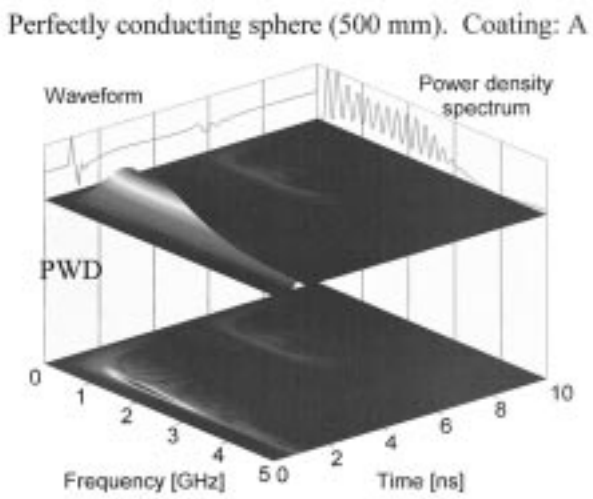

Fig. 11. Surface plot and its plane projection intensity image of the PWD together with the returned waveform and its power density spectrum when a perfectly conducting sphere covered with coating A is illuminated in monostatic mode by the designed incident pulse.

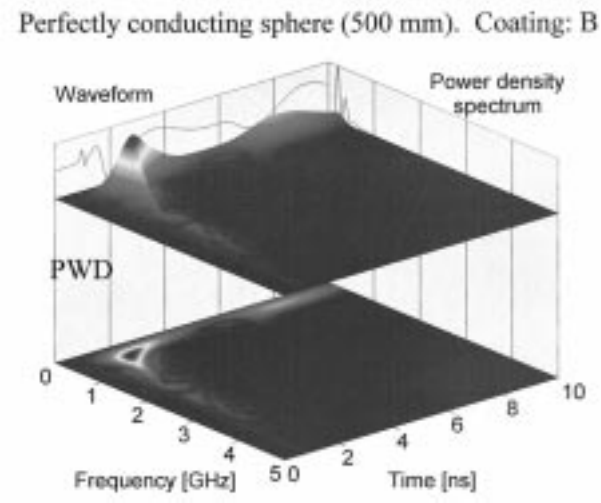

Fig. 12. Surface plot and its plane projection intensity image of the PWD together with the returned waveform and its power density spectrum when a perfectly conducting sphere covered with coating B is illuminated in monostatic mode by the designed incident pulse.

sphere covered with the nonmagnetic lossy dielectric "A," and in Figs. 17 and 18 for the sphere covered with the magnetic coating layer "B." Figs. 13, 15, and 17 pertain to the E-plane scattering, and Figs. 14, 16, and 18 to the H-plane scattering cases. These bistatic (normalized) cross-sections as defined by (18) are represented in an arbitrary color scale (pseudocolors) graded from dark blue (0), through shades of magenta, green, yellow, and red, to brown (3 and higher levels). The direction of wave incidence is always from the left (i.e., $\theta = 0°$) of the plots. The outer radius of the bare sphere is $a = 250$ mm and the thickness of the coating is always 5 mm, making the outer radius for the coated spheres $a = 255$ mm. The frequency scale is displayed in the radial direction and it ranges in gigahertz units from 0 at the center to 5 at the outermost circle shown.

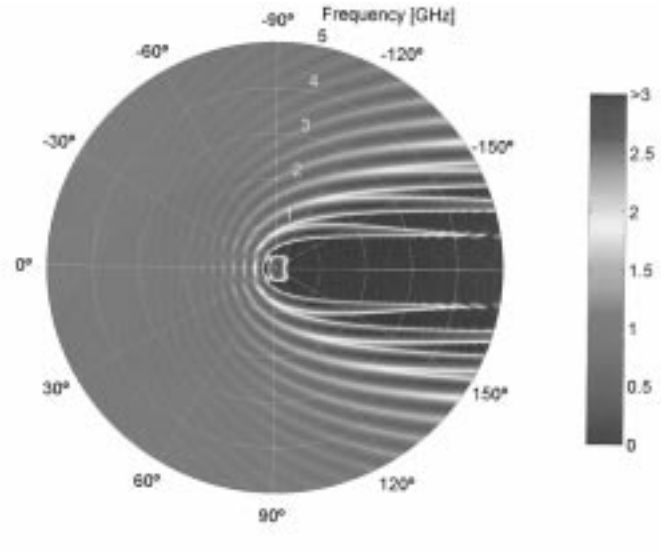

Fig. 13. Bistatic radar cross section (RCS) for an uncoated perfectly conducting sphere of radius $a = 250$ mm. For the E-plane scattering case.

This is equivalent to 5.2 (nondimensional) ka-values per circle, up to $ka \approx 26$ at the outermost circle.

Cross-section levels considerably higher than 3 occur in the forward scattering direction (i.e., $\theta = 180°$) for all three targets, coated or not. However, the forward scattered power is usually 180° out of phase with the incident field, and forms, when added to the incident field, a shadow region behind the scattering object [2]. Away from the forward scattering direction there are noticeable differences in the cross-sections displayed in Figs. 13–18. For the uncoated sphere (see Figs. 13 and 14) there are fringes of higher and lower values that are more noticeable in Fig. 13 (E-plane case) than in Fig. 14 (H-plane case). These values oscillate about the unit value and are due to constructive or destructive interference between the specularly reflected wave in a given direction and the creeping wave that radiates off the target in the same direction. As it should be, there is no difference between the two scattering cases (i.e., E- and H-plane) in the monostatic backscattering direction (i.e., $\theta = 0$) since the two cases are here identical. The fringe pattern in this direction indicates the graduated weakening of the scattering amplitudes in agreement with Fig. 2 (i.e., about four fringes per gigahertz division). One apparent result of this bistatic analysis is that the occurrence of noticeable signature features in the frequency domain depend in general on the polarization of the incident waveform.

For the sphere with coating "A" and away from the forward scattering direction, there are about a dozen color fringes oscillating about a unit value up to a frequency of 3 GHz, again more clearly visible in the E-plane case (Fig. 15) than in the H-plane case (Fig. 16). For higher frequencies there occurs a substantial decrease to very low values of the cross-section at about 4 GHz followed by increasing values for yet higher frequencies. This agrees with the low dip this coating introduces in the monostatic backscattering ($\theta = 0$) case, as seen in Fig. 4. The dozen fringes seen correspond to the curvature-induced oscillations present in Fig. 4 for

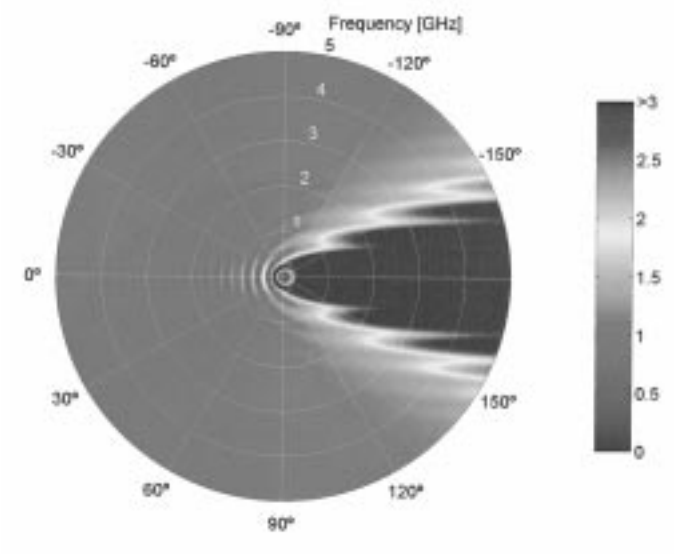

Fig. 14. Same as Fig. 13, but for the H-plane scattering case.

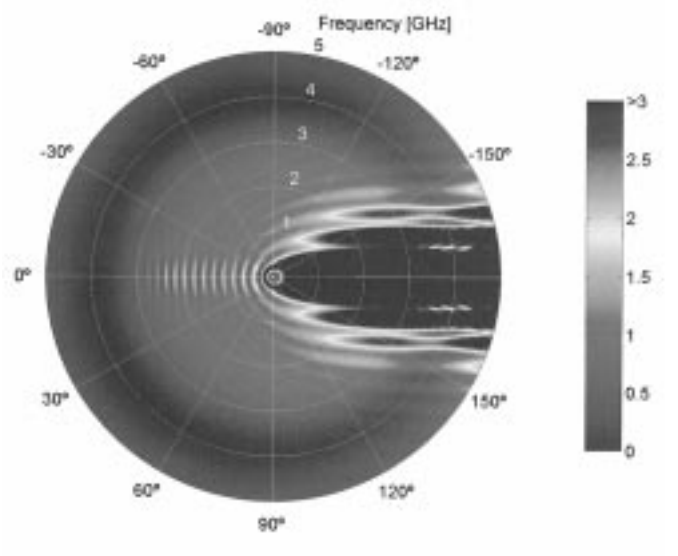

Fig. 16. Same as Fig. 15, but for the H-plane scattering case.

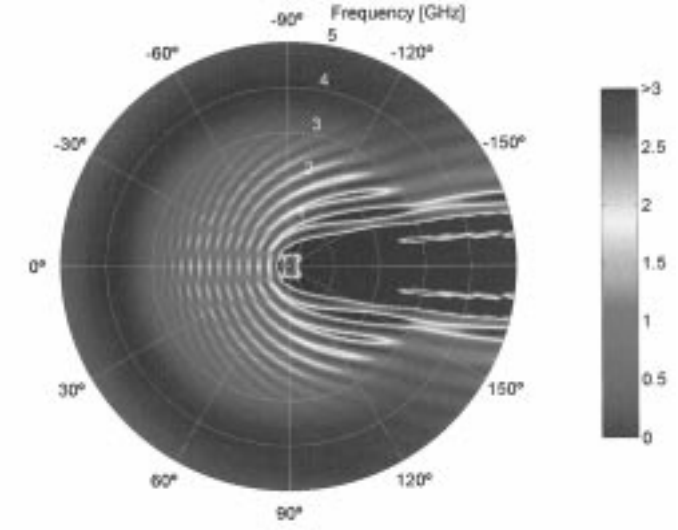

Fig. 15. Bistatic RCS for a perfectly conducting sphere of radius $a = 250$ mm covered with the (nonmagnetic) coating "A." For E-plane scattering.

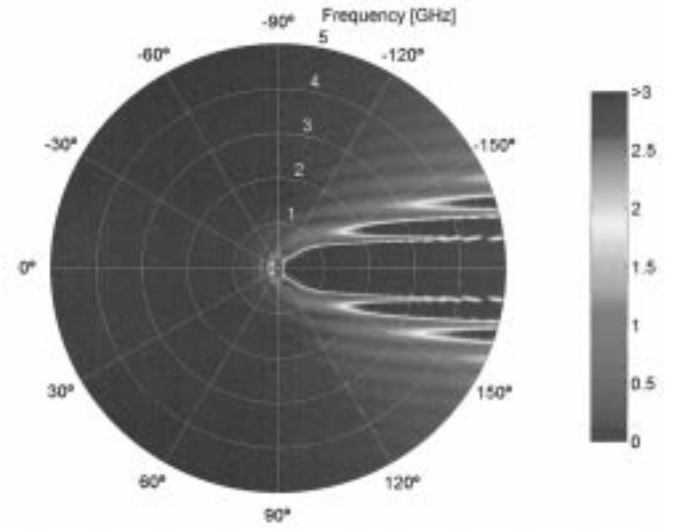

Fig. 17. Bistatic RCS for a perfectly conducting sphere of radius $a = 250$ mm covered with the magnetic coating B described in the text. For E-plane scattering.

backscattering and its vicinity. For the sphere covered with the magnetic coating "B" we see that the scattering amplitudes are practically zero (dark blue) almost everywhere away from the forward scattering direction (see Figs. 17 and 18). In the backscattering direction ($\theta = 0$) this is in agreement with Fig. 7, particularly above 1 GHz. In brief, the most effective coating is "B"; it is the most broad band and it is effective down to frequencies of 1 GHz. The region below 1 GHz for backscattering is the only one showing relatively high amplitudes, which agrees with the findings in Fig. 12. Only at low frequencies that strong RCS values are observed and we note in particular that those values occur for a larger range of the bistatic angle in the H-plane case (Fig. 18). Hence, even when one has such an effective coating above 1 GHz, high-resonance scattering amplitudes then appearing at lower frequencies can be used for target identification purposes [20], [21] and for a wider range of the bistatic angle using H-plane scattering.

VI. Conclusions

We have studied the scattering interactions present when a waveform is incident on a few targets of simple shape in the traditional frequency and time domains and also in the combined time-frequency domain using a pseudo-Wigner distribution. In the latter case, the waveform incident on the targets was a short ultrawide-band pulse resulting from a filter design technique we developed earlier. We have demonstrated the close relation between the backscattering RCS of a simple target and the power reflection coefficient of an infinite flat plate at normal incidence when both are covered with the same type of coating made of a microwave absorbing material. We have also demonstrated the distinctive differences in both those target responses that are present at low frequencies.

Comparing the PWD's of a simple-shaped target without any coating or with one of two different applied coatings

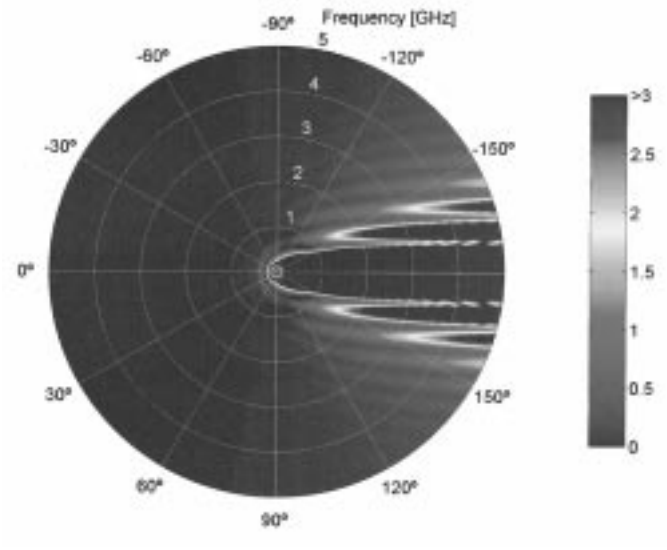

Fig. 18. Same as Fig. 17, but for the H-plane scattering case.

clearly demonstrated that the coating itself, although reducing the RCS, could induce additional resonance features in the target's signature at low frequencies. If extracted by a suitable radar, those low-frequency features can be used for target recognition purposes. It also follows from our analysis that an absorbing coating would also make high-frequency resonance features negligible even when there is only a small amount of absorption present.

Finally, a study of bistatic RCS of these bare and coated objects confirms the above observations extracted from the PWD plots in Figs. 10–12. It further permits the quantitative display of the angular (sectors) and frequency (annular) regions in which the cross-sectional features of interest appear. Although these features are reduced in some regions, they are enhanced in others and, thus, this behavior becomes the tool to be used for identification of coated targets [21], [22].

ACKNOWLEDGMENT

The authors would like to thank the Independent Research Boards of their respective institutions for their support.

REFERENCES

[1] G. T. Ruck, D. E. Barrick, W. D. Stuart, and C. K. Krichbaum, *Radar Cross Section Handbook.* New York: Plenum, 1970, vol. 1.

[2] E. F. Knott, J. F. Shaeffer, and M. T. Tuley, *Radar Cross Section*, 2nd ed. Norwood, MA: Artech House, 1993.

[3] W. H. Press, B. P. Flannery, S. A. Teukolsky, and W. T. Vetterling, *Numerical Recipes: The Art of Scientific Computing.* New York: Cambridge Univ. Press, 1986.

[4] A. L. Aden and M. Kerker, "Scattering of electromagnetic waves from two concentric spheres," *J. Appl. Phys.*, vol. 22, pp. 1242–1246, Oct. 1951.

[5] J. Rheinstein, "Scattering of electromagnetic waves from dielectric coated conducting spheres," *IEEE Trans. Antennas Propagat.*, vol. 12, pp. 334–340, May 1964.

[6] G. Gaunard, H. Überall, and P. J. Moser, "Resonances of dielectrically coated spheres and the inverse scattering problem," *J. Appl. Phys.*, vol. 52, pp. 35–43, Jan. 1981.

[7] G. C. Gaunard, H. C. Strifors, and W. H. Wertman, "Transient effects in the scattering of arbitrary EM pulses by dielectric spherical targets," *J. Electromagn. Waves Applicat.*, vol. 5, pp. 75–92, Jan. 1991.

[8] H. T. Kim, "High-frequency analysis of EM scattering from a conducting sphere coated with a composite material," *IEEE Trans. Antennas Propagat.*, vol. 41, pp. 1665–1674, Dec. 1993.

[9] H. C. Strifors, S. Abrahamson, B. Brusmark, and G. C. Gaunard, "Bistatic scattering by a spherical dielectric target illuminated by an electromagnetic pulse," in *Automat. Object Recogn. III—Proc. SPIE*, F. A. Sadjadi, Ed., vol. 1960, pp. 2–13, 1993.

[10] H. C. Strifors, G. C. Gaunard, B. Brusmark, and S. Abrahamson, "Transient interactions of an EM pulse with a dielectric spherical shell," *IEEE Trans. Antennas Propagat.*, vol. 42, pp. 453–462, Apr. 1994.

[11] H. C. Strifors and G. C. Gaunard, "Scattering of short, ultra-wideband electromagnetic pulses by simple targets with reduced radar cross-section," in *Ultra-Wideband, Short-Pulse Electromagnetics 2*, L. Carin and L. B. Felsen, Eds. New York: Plenum Press, 1995, pp. 447–454.

[12] L. Cohen, "Time-frequency distribution—A review," *Proc. IEEE*, vol. 77, pp. 941–981, July 1989.

[13] ———, *Time-Frequency Analysis.* Englewood Cliffs, NJ: Prentice-Hall, 1995.

[14] T. A. C. M. Claasen and W. F. G. Mecklenbräuker, "The Wigner distribution—A tool for time-frequency signal analysis," *Philips J. Res.*, vol. 35, pt. I, pp. 217–250; pt. II, pp. 276–300; pt. III, pp. 372–389, 1980.

[15] W. J. Lentz, "Generating Bessel functions in Mie scattering calculations using continued fractions," *Appl. Opt.*, vol. 15, pp. 668–671, Mar. 1976.

[16] ———, "Continuous fraction calculation of spherical Bessel functions," *Comput. Phys.*, vol. 4, pp. 403–407, July/Aug. 1990.

[17] M. Abramowitz and I. A. Stegun, Eds., *Handbook of Mathematical Functions.* Washington, DC: U.S. Govt. Printing Office, 1972.

[18] E. M. Kennaugh and D. L. Moffatt, "Transient and impulse response approximations," *Proc. IEEE*, vol. 53, pp. 893–901, Aug. 1965.

[19] A. V. Oppenheim and R. W. Schafer, *Digital Signal Processing.* Englewood Cliffs, NJ: Prentice-Hall, 1975.

[20] R. E. Hiatt, K. M. Siegel, and H. Weil, "The ineffectiveness of absorbing coatings on conducting objects illuminated by long wavelength radar," *Proc. IRE*, vol. 48, pp. 1636–1642, 1960.

[21] G. C. Gaunard and H. C. Strifors, "Signal analysis by means of time-frequency (Wigner-type) distributions—Applications to sonar and radar echoes," *Proc. IEEE*, vol. 84, pp. 1231–1248, Sept. 1996.

[22] ———, "Transient resonance scattering and target identification," *Appl. Mech. Rev.*, vol. 50, pp. 131–148, Mar. 1997.

[23] G. C. Gaunard, D. Brill, H. Huang, P. W. Moore, and H. C. Strifors, "Signal processing of the echoe-signatures returned by submerged shells insonified by dolphin "clicks": Active classification," *J. Acoust. Soc. Amer.*, vol. 103, pp. 1547–1557, Mar. 1998 (acoustic/sonar example).

Hans C. Strifors (M'91) received the Ph.D. degree in solid mechanics from the Royal Institute of Technology, Stockholm, Sweden, in 1974.

He held positions at the Royal Institute of Technology, where his research activities included continuum mechanics, fracture, and plasticity. In 1982, he joined the Division of Materials Research, of the Defense Research Establishment (FOA), Stockholm. In recent years he has specialized in electromagnetic and acoustic scattering theory. His professional interests include the scattering interaction of electromagnetic, acoustic, and elastic waves with lossy an lossless materials and structures. He presently carries on research programs on control of electromagnetic properties of materials and structures, radar and sonar scatterings, and the application of digital signal processing to target identification. Over the years, he has been the author or coauthor of numerous journal and conference papers in the areas of mechanics, acoustics, and electromagnetism.

Dr. Strifors is a Member of the Acoustical Society of America and the New York Academy of Sciences.

Guillermo C. Gaunaurd (M'82–SM'83) received the B.A. (mathematics), B.S.M.E, M.S., and Ph.D. (physics/acoustics) degrees from Catholic University, Washington, DC, in 1964, 1966, 1967, and 1971, respectively.

He is a Senior Research Physicist at the Carderock Division of the Naval Surface Warfare Center (N.S.W.C.), Bethesda, MD, where he is currently a Group Leader in the Weapons Materials Department. He has been with N.S.W.C. since 1971, specializing on the scattering interaction of acoustic, electromagnetic, and elastic waves with materials and structures. His research over the years has mainly dealt with radiation and scattering problems of classical physics, mechanics of deformable media, fluid-structure interactions, electromagnetic theory, and applied mathematics. He is the author/coauthor of more than 120 scientific journal articles and more than 300 other publications and/or presentations at professional societies, congresses, symposia, and government reports. He has delivered scores of invited papers/keynote lecturers at scientific meetings and universities. He has organized/chaired dozens of special technical sessions and entire scientific conferences. He lectured intermittently (part time) at the Engineering School of the University of Maryland, College Park. He holds four patents.

Dr. Gaunaurd has won a number of awards including the Washington Academy of Sciences "Scientific Achievement Award" (1989), the National Defense Preparedness Society Bronze Medal (1991), and others within N.S.W.C. His professional biography is listed in *American Men of Science*, *Who's Who in America*, and a dozen other such books. He has been a Guest Editor of the IEEE JOURNAL OF OCEANIC ENGINEERING and since 1992 has been an Associate Editor of the IEEE TRANSACTIONS ON ULTRASONICS, FERROELECTRICS AND FREQUENCY CONTROL. He is a member of several scientific societies including the New York Academy of Sciences, Sigma Xi, The American Academy of Mechanics, Washington's Society of Engineers, and the International Union of Mathematical Physics. He is a Fellow of the Acoustical Society of America, the American Society of Mechanical Engineers, and the Washington Academy of Sciences.